Metrol. Meas. Syst., Vol. 26 (2019) No. 4, pp. 617–629
DOI: 10.24425/mms.2019.130566

METROLOGY AND MEASUREMENT SYSTEMS
Index 330930, ISSN 0860-8229
www.metrology.pg.gda.pl

ROTARY UPGRADING METHOD AND ITS EXPERIMENTAL STUDY OF AN INERTIALLY STABILIZED PLATFORM

Rong Guo[1,2)], Xueyun Wang[1)], Jingjuan Zhang[1)], Tianxiao Song[1)]

1) *Beihang University, School of Instrumentation Science and Opto-electronics Engineering, Beijing 100191, China* (✉ *guorong633@buaa.edu.cn*, +86 10 8233 9270, *wangxueyun@buaa.edu.cn*, *zhangjingjuan@buaa.edu.cn*, *songtianxiao_buaa@126.com*)
2) *North University of China, School of Information and Communication Engineering, Taiyuan 030051, China*

Abstract

Rotation modulation can significantly improve the navigation accuracies of an inertial navigation system (INS) and a strap-down configuration dominating in this type of INS. However, this style of construction is not a good scheme since it has no servo loop to counteract a vehicle manoeuvre. This paper proposes a rotary upgrading method for a rotational INS based on an inertially stabilized platform. The servo control loop is reconstructed on a four-gimbal platform, and it has the functions of providing both a level stability relative to the navigation frame and an azimuth rotation at a speed of 1.2°/s. With the platform's rotation, the observability and the convergence speed of the estimation for the initial alignment can be improved, as well as the biases of the gyroscopes and accelerometers be modulated into zero-mean periodic values. An open-loop initial alignment method is designed, and its detailed algorithms are delivered. The experiment result shows that the newly designed rotational INS has reached an accuracy of 0.38 n mile/h (CEP, circular error probable). The feasibility and engineering applicability of the designed scheme have been validated.

Keywords: inertially stabilized platform (ISP), rotation modulation, four-gimbal platform, servo control, initial alignment.

1. Introduction

An *inertially stabilized platform* (ISP) is a mechanism, typically involving gimbal assemblies, for controlling the inertial orientation of its payload [1, 2]. It is one of the core components of an inertial navigation system. *Inertial navigation systems* (INSs) are self-contained, non-radiating, dead-reckoning navigation systems, and their position error propagations unfortunately grow with time because of gyroscope drifts and accelerometer biases [3–5]. To design a high performance INS, a growing number of *rotational INSs* (RINSs) have been researched because the technology of rotation modulation is an effective method for enhancing the accuracy of an INS by modulating the gyroscope drift and accelerometer bias errors into zero-mean periodically varying components [6–10]. The Delco Carousel *inertial measurement unit* (IMU) in the Titan IIIC vehicle is the type

of its application, which has two sets of inertial instruments mounted on a platform that rotates at 1 rpm around an inertially fixed axis. However, there are two obvious disadvantages of the Delco Carousel IMU. One disadvantage is that this system needs additional hardware in the turret to implement rotation. The other disadvantage is that the system does not adopt an alignment method that is suitable for rotation. In addition, rotation modulation is also applied to the strap-down system. For instance, Litton Inc. designed an AN/WSN-5L system being rotated 720° clockwise around the azimuth axis and then rotated 720° counter-clockwise. In references therein, there are some applications illustrating an INS that has been rotated around one or two rotational axes according to specific rules and that has had its navigation accuracy effectively improved [3, 9–11]. However, when a vehicle is influenced by angular motion, the auto compensation may be degraded. The reason for this is that the angular motion, coupled with the scale factor and the installation error, can reduce the precision of the INS and produce a new type of error [4, 11].

There will be significant application prospects if the INS could apply not only the technology of rotation modulation but also isolate a vehicle's angular motion using a stabilized platform. A feasible and effective method to accomplish this is to upgrade the existing platform INS to a rotational INS. In the process, the design is focused on the servo control loop and the initial alignment because they directly determine the performance of the rotational INS. The servo control loop needs to process the analogue signal with a digital circuit and a conversion component and to keep the platform rotation continuous with the azimuth axis and levelly stabilized at the same time [12–17]. As the key technology of the INS, the initial alignment aims to calculate the misalignment angles between the platform frame (p-frame) and the local geographic frame (t-frame), and then to level the platform and align the p-frame with the t-frame, or to obtain a coordinate transformation matrix describing transforming the body frame (b-frame) to the t-frame [18–21]. Hence, the accuracy and rapidity of the initial alignment have a major impact on the performance of the INS. In references [19–27], such alignment methods as a dimensionality reduction Gauss–Hermite filter [23] and a Kalman filter [24, 25] were proposed to implement fine alignment. In reference [26], an optimization-based alignment approach was proposed, and an attitude alignment was equivalently transformed into a "continuous" attitude determination problem. The existing research on alignment methods is focused mainly on strap-down systems while platform-based rotational INSs are still seldom considered.

This paper is focused on the designing and implementing a rotational INS and illustrates it based on a four-gimbal platform. It can be seen as a rotary upgrading method for adopting the technology of rotation modulation to an ISP. A complete design procedure of the servo control loop and initial alignment algorithms are presented in Section 2. Section 3 describes the system configuration. Section 4 presents a set of experiments carried out to assess the effectiveness of the proposed method. The conclusion is provided at the end of the paper.

2. Rotary upgrading method

We have selected a four-gimbal inertially stabilized platform, which was originally designed and used by aircraft; such a platform can be considered as the research foundation and be upgraded to a new rotational platform INS with a much better navigation accuracy. The navigation accuracy of the original system is 2 n mile/h *circular error probable* (CEP) and the alignment accuracy is 9′. A photo of the platform is shown in Fig. 1.

A pair of two-degree-of-freedom *dynamically tuned gyroscopes* (DTGs) and three accelerometers are orthogonally mounted on the innermost gimbal. The accuracy of gyroscope is 0.03°/h and the accuracy of accelerometer is 100 μg. The order of gimbals elements from the inner to

Metrol. Meas. Syst., Vol. 26 (2019), No. 4, pp. 617–629
DOI: 10.24425/mms.2019.130566

Fig. 1. The physical structure of the four-gimbal platform.

the outer is: the azimuth gimbal (a-gimbal), the inner roll gimbal (q-gimbal), the pitch gimbal (p-gimbal), and the outer roll gimbal (r-gimbal). Each gimbal axis has a torque motor and a resolver directly coupled to the two adjacent members without operating through a gear train. The gimbals angle is the relative angle between the inner gimbal and the outer gimbal, which is measured by the corresponding resolver. The motion of a gimbal is driven by its corresponding torque motor.

2.1. Servo control loop

2.1.1. Principle of control loop

The servo control loop is responsible for holding the t-frame steady irrespective of changes in attitude or the heading of the vehicle. According to the characteristics of a four-gimbal platform, there are four control loops that need to be designed. Among them, the azimuth gimbal control loop also needs to drive the platform to rotate along with the z-axis of the t-frame continuously. A block diagram of the control loop is shown in Fig. 2.

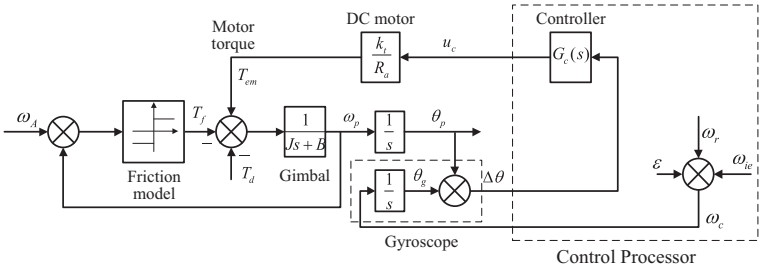

Fig. 2. A block diagram of the control loop.

The vehicle experiences an angular velocity ω_A, which leads to an inertial platform angular movement caused by the bearing friction T_f. The angular velocity of inertial platform ω_p acts on the gimbal by the friction torque and the torque disturbance T_d. The inertial element consists of the moment of inertia about the gimbal J and the coefficient of viscous friction B. The size and direction of any deviation of the stabilized platform from its reference orientation is given by the error angle $\Delta\theta$. The controller $G_c(s)$ calculates the corresponding control voltage u_c. The gimbal drive motor, which is represented by the moment coefficient k_t and the armature resistance R_a,

generates a torque T_{em} to reject the disturbance torque T_d. Another function of the stabilized platform is the rotation of the platform. The processor calculates the angular velocity command, which consists of the gyroscope drift ε, the earth rate components, and the rotation rate ω_r. At the same time, the torque current is calculated in order to produce the gyroscope precession and the precession angle θ_g. Accordingly, the gyroscope pickoff angle $\Delta\theta$ is produced. As a result, the control voltage u_c is calculated using the controller $G_c(s)$ and applied to the motor in order to drive the platform rotation. The parameters of the four control loops are listed in Table 1. The indexes a, q, p and r denote the azimuth, inner roll, pitch and outer roll gimbal, respectively.

Table 1. Parameters of the control loop.

Moment of inertia	Values ($\mathrm{kg{\cdot}m^2}$)	Moment coefficient	Values (N·m/A)	Armature resistent	Values (Ω)
J_a	0.0026	k_{ta}	0.21	R_a	31.2
J_q	0.0066	k_{tq}	0.21	R_q	35.5
J_p	0.0093	k_{tp}	0.21	R_p	28.7
J_r	0.0115	k_{tr}	0.29	R_r	34.3

2.1.2. Control signal

Figure 3 shows the topological structure of the gimbals and platform, from which the control signal can be calculated. The variables A_x, A_y, A_z denote the output signals of accelerometers, X_g, Y_g, X_g' denote the output signals of gyroscope pickoff, H denotes the spin axis of gyroscope.

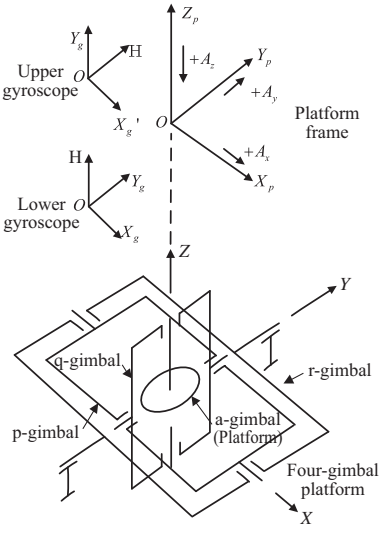

Fig. 3. The topological structure of the platform.

The precession torque in the horizontal direction is developed from the lower gyroscope, and the signals X_g and Y_g drive the horizontal gimbal motors. The precession torque in the azimuth direction is developed from the upper gyroscope, and the signal Y_g drives the azimuth gimbal

Metrol. Meas. Syst., Vol. 26 (2019), No. 4, pp. 617–629
DOI: 10.24425/mms.2019.130566

motor. Another signal X'_g is used to achieve the platform lock. The outer-roll gimbal is a redundant gimbal that keeps the inner-roll gimbal at the null value. And its control signal is the inner-roll gimbal angle. The variables $\Delta\theta_{am}$, $\Delta\theta_{qm}$, $\Delta\theta_{pm}$, $\Delta\theta_{rm}$ denote the control signals of each gimbal loop. Then:

$$\begin{pmatrix} \Delta\theta_{pm} \\ \Delta\theta_{qm} \\ \Delta\theta_{am} \end{pmatrix} = C_p^t \begin{pmatrix} \Delta\theta_{gx} \\ \Delta\theta_{gy} \\ \Delta\theta_{gz} \end{pmatrix} = \begin{pmatrix} \cos\theta_a & -\sin\theta_a & 0 \\ \sin\theta_a & \cos\theta_a & 0 \\ 0 & 0 & 1 \end{pmatrix} \begin{pmatrix} \Delta\theta_{gx} \\ \Delta\theta_{gy} \\ \Delta\theta_{gz} \end{pmatrix}, \tag{1}$$

$$\Delta\theta_{rm} = \frac{\theta_q}{\cos\theta_p} = \theta_q \sec\theta_p \,,$$

where C_p^t denotes the coordinate transformation matrix between t-frame and p-frame. $\Delta\theta_{gx}$, $\Delta\theta_{gy}$ and $\Delta\theta_{gz}$ are the platform dip angles that are detected by gyroscope pickoff. θ_a, θ_q, θ_p and θ_r are the gimbal angles that are sensed by the gimbal resolver.

The rotation can be achieved by the computer's supplied pulse into the torqueing circuit. The current is then fed into the gyroscope torque unit. The rotation command angular velocity of the platform is calculated according to the following formula:

$$\omega_c = C_t^p \left(\varepsilon_g + \omega_{it}^t + \omega_r\right), \tag{2}$$

where:

$$\begin{bmatrix} \omega_{cx} \\ \omega_{cy} \\ \omega_{cz} \end{bmatrix} = \begin{bmatrix} \varepsilon_{gx} \\ \varepsilon_{gy} \\ \varepsilon_{gz} \end{bmatrix} + \begin{pmatrix} \cos\varphi_z & \sin\varphi_z & 0 \\ -\sin\varphi_z & \cos\varphi_z & 0 \\ 0 & 0 & 1 \end{pmatrix} \begin{bmatrix} \omega_{itx}^t \\ \omega_{ity}^t \\ \omega_{itz}^t \end{bmatrix} + \begin{bmatrix} \omega_{rx} \\ \omega_{ry} \\ \omega_{rz} \end{bmatrix}. \tag{3}$$

$(\varepsilon_{gx}\ \varepsilon_{gy}\ \varepsilon_{gz})$ represents the gyroscope drift, $(\omega_{rx}\ \omega_{ry}\ \omega_{rz})$ represents the rotation speed, and $(\omega_{gx}^t\ \omega_{gy}^t\ \omega_{gz}^t)$ is the earth rate component, and:

$$\begin{bmatrix} \omega_{itx}^t \\ \omega_{ity}^t \\ \omega_{itz}^t \end{bmatrix} = \begin{bmatrix} -\dfrac{V_{yt}}{R_{yt}} \\ \omega_{ie}\cos L + \dfrac{V_{xt}}{R_{xt}} \\ \omega_{ie}\sin L + \dfrac{V_{xt}}{R_{xt}}\tan L \end{bmatrix}, \tag{4}$$

where: V_{yt}; V_{xt}; R_{yt} and R_{xt} are, respectively, the north velocity, the east velocity, the radius of curvature of the meridian, and the radius of curvature of the meridian in the prime vertical.

2.2. Initial alignment method

In the initial alignment stage, the platform enters the rotating state and rotates bi-directionally along the z-axis in one circle. By establishing the mathematical model of fine alignment, the outputs of the accelerometers can be introduced as measurement variables. The test data can be calculated with the recursive least-square method in order to estimate the state variables, such as misalignment angles, accelerometer bias, and gyroscope drifts.

2.2.1. Mathematical model

Ignoring the position and velocity errors, the misalignment angle error equation of the INS platform on the stationary base can be written as follows:

$$\begin{cases} \delta\dot{\phi}_E = \delta\phi_N\omega_U - \delta\phi_U\omega_N + \varepsilon_E \\ \delta\dot{\phi}_N = -\delta\phi_E\omega_U + \varepsilon_N \\ \delta\dot{\phi}_U = \delta\phi_E\omega_N + \varepsilon_U \end{cases}, \tag{5}$$

where: ω is the earth rate; ε is the gyroscope drift; and the subscripts E; N; and U represent the projection of variables along the east, north, and up directions, respectively.

The analytical expression of the misalignment angle can be obtained as follows:

$$\begin{cases} \delta\phi_E(t) = \delta\phi_{E0}\cos\omega_{ie}t + \dfrac{\varepsilon_E - \delta\phi_{U0}\omega_N + \delta\phi_{N0}\omega_U}{\omega_{ie}}\sin\omega_{ie}t \\ \qquad + \dfrac{\varepsilon_N\omega_U - \varepsilon_U\omega_N}{\omega_{ie}^2}(1-\cos\omega_{ie}t) \\ \delta\phi_N(t) = \delta\phi_{N0} + \varepsilon_N t - \dfrac{\varepsilon_E - \delta\phi_{U0}\omega_N + \delta\phi_{N0}\omega_N}{\omega_{ie}^2}\omega_U(1-\cos\omega_{ie}t) \\ \qquad - \dfrac{\varepsilon_N\omega_U - \varepsilon_U\omega_N}{\omega_{ie}^2}\omega_U\left(t - \dfrac{1}{\omega_{ie}}\sin\omega_{ie}t\right) - \dfrac{\delta\phi_{E0}\omega_U}{\omega_{ie}}\sin\omega_{ie}t \end{cases}, \tag{6}$$

where: $\delta\phi_{E0}$; $\delta\phi_{N0}$ and $\delta\phi_{U0}$ represent the initial values of the misalignment angles. Since the alignment time is much shorter than the period of the rotation of the earth, we can make the approximation:

$$\begin{cases} \sin\omega_{ie}t \approx \omega_{ie}t \\ \cos\omega_{ie}t \approx 1 \end{cases}. \tag{7}$$

Then, (6) reduces to:

$$\begin{cases} \delta\phi_E(t) = \delta\phi_{E0} + (-\omega_N\delta\phi_{U0} + \omega_U\delta\phi_{N0})t \\ \delta\phi_N(t) = -\omega_U\delta\phi_{E0}t + \delta\phi_{N0} + \varepsilon_N t \end{cases}. \tag{8}$$

In the non-rotation mode, the accelerometer biases are ∇_x and ∇_y. Then, (8) becomes:

$$\begin{cases} \Delta\phi_E = \Delta\phi_{E0} + \dfrac{\nabla_y}{g} + (-\omega_N\Delta\phi_{U0} + \omega_U\Delta\phi_{N0})t \\ \Delta\phi_N = -\omega_U\Delta\phi_{E0}t + \Delta\phi_{N0} - \dfrac{\nabla_x}{g} + \varepsilon_N t \end{cases}. \tag{9}$$

Due to the coupling relationship between the initial values of the misalignment angles and the accelerometer biases, the errors cannot be separated from the misalignment angles. During the platform's rotation along the z_t axis, the relationship between s-frame and t-frame can be defined by the rotation angle φ_z. ω_r is the rotation rate, and $\varphi_z = \omega_r t$. The accelerometer biases are modulated into the periodic form by a matrix describing transformation the s-frame to the n-frame. Then, (9) can be rewritten as:

$$\begin{cases} \Delta\phi_E = \Delta\phi_{E0} + \dfrac{\nabla_y}{g}\cos\omega_r t + \dfrac{\nabla_x}{g}\sin\omega_r t + (-\omega_N\Delta\phi_{U0} + \omega_U\Delta\phi_{N0})t \\ \Delta\phi_N = -\omega_U\Delta\phi_{E0}t + \Delta\phi_{N0} - \dfrac{\nabla_x}{g}\cos\omega_r t + \dfrac{\nabla_y}{g}\sin\omega_r t + \varepsilon_N t \end{cases}. \tag{10}$$

Metrol. Meas. Syst., Vol. 26 (2019), No. 4, pp. 617–629
DOI: 10.24425/mms.2019.130566

It can be seen that the accelerometer biases are separated from the coupling, and the errors can be estimated from the misalignment angles, so the observable degree can clearly be improved, and the convergence speed can be reduced. Similarly, the horizontal equivalent gyroscope drift in the n-frame can be written as:

$$\begin{cases} \varepsilon_E = \varepsilon_x \cos\omega_r t - \varepsilon_y \sin\omega_r t \\ \varepsilon_N = \varepsilon_x \sin\omega_r t + \varepsilon_y \cos\omega_r t \end{cases}. \tag{11}$$

The misalignment angle in rotation can be calculated as follows:

$$\begin{cases} \Delta\phi_E = \int\limits_0^t \varepsilon_E dt = \dfrac{(\varepsilon_x \sin\omega_r t + \varepsilon_y \cos\omega_r t)}{\omega_r} - \dfrac{\varepsilon_y}{\omega_r} \\ \Delta\phi_N = \int\limits_0^t \varepsilon_N dt = \dfrac{(-\varepsilon_x \cos\omega_r t + \varepsilon_y \sin\omega_r t)}{\omega_r} + \dfrac{\varepsilon_x}{\omega_r} \end{cases}. \tag{12}$$

Thus, the resulting state equation of the misalignment angle can be written as:

$$\begin{cases} \Delta\phi_E = \Delta\phi_{E0} + (-\omega_N \Delta\phi_{U0} + \omega_U \Delta\phi_{N0})t \\ \qquad + \sin\varphi_z \dfrac{\nabla_x}{g} + \cos\varphi_z \dfrac{\nabla_y}{g} + \sin\varphi_z \dfrac{\varepsilon_x}{\omega_r} + (\cos\varphi_z - 1)\dfrac{\varepsilon_y}{\omega_r} \\ \Delta\phi_N = \Delta\phi_{N0} + \varepsilon_N t - \omega_U \Delta\phi_{E0} t \\ \qquad - \cos\varphi_z \dfrac{\nabla_x}{g} + \sin\varphi_z \dfrac{\nabla_y}{g} - (\cos\varphi_z - 1)\dfrac{\varepsilon_x}{\omega_r} + \sin\varphi_z \dfrac{\varepsilon_y}{\omega_r} \end{cases}. \tag{13}$$

2.2.2. LSQ for estimation

The observation equation can be given by:

$$Z = HX + V, \tag{14}$$

where: Z is the observation vector; H is the observation matrix; V is the noise vector. Due to the coupling effect, the east gyroscope drift is unobservable, so the state variable X is set as:

$$X = \begin{bmatrix} \delta\phi_{E0} & \delta\phi_{N0} & \delta\phi_{U0} & \varepsilon_N & \nabla_x & \nabla_y & \varepsilon_x & \varepsilon_y \end{bmatrix}^T. \tag{15}$$

The observation matrix is then written as:

$$H = \begin{bmatrix} 1 & \omega_U t & -\omega_N t & 0 & \dfrac{\cos\varphi_z}{g} & \dfrac{-\sin\varphi_z}{g} & \dfrac{\sin\varphi_z}{\omega_r} & \dfrac{\cos\varphi_z - 1}{\omega_r} \\ -\omega_U t & 1 & 0 & t & \dfrac{\sin\varphi_z}{g} & \dfrac{\cos\varphi_z}{g} & \dfrac{1 - \cos\varphi_z}{\omega_r} & \dfrac{\sin\varphi_z}{\omega_r} \end{bmatrix}. \tag{16}$$

The horizontal platform misalignment angles are selected as the external reference, so the observation vector is computed as follows:

$$Z = \begin{bmatrix} \Delta\phi_E \\ \Delta\phi_N \end{bmatrix} = \begin{bmatrix} \nabla_N/g \\ -\nabla_E/g \end{bmatrix} = \begin{bmatrix} 0 & 1/g \\ -1/g & 0 \end{bmatrix} \begin{bmatrix} \cos\varphi_z & -\sin\varphi_z \\ \sin\varphi_z & \cos\varphi_z \end{bmatrix} \begin{bmatrix} \nabla_x \\ \nabla_y \end{bmatrix}. \tag{17}$$

The recursive *least square* (LSQ) method is chosen to estimate the error parameters of X, and the equation is written as:

$$\begin{cases} \boldsymbol{P}_{k+1} = \boldsymbol{P}_k - \boldsymbol{P}_k \boldsymbol{H}_{k+1}^T \left(\boldsymbol{I} + \boldsymbol{H}_{k+1} \boldsymbol{P}_k \boldsymbol{H}_{k+1}^T \right)^{-1} \boldsymbol{H}_{k+1} \boldsymbol{P}_k \\ \hat{\boldsymbol{X}}_{k+1} = \hat{\boldsymbol{X}}_k - \boldsymbol{P}_{k+1} \boldsymbol{H}_{k+1}^T \left(\boldsymbol{Z}_{k+1} - \boldsymbol{H}_{k+1} \hat{\boldsymbol{X}}_k \right) \end{cases}, \tag{18}$$

where: I is the identity matrix; the initial of X is the zero vector and the initial of P is the identity matrix. At the end of the fine alignment, the deterministic torqueing rate for each gyroscope consists of the earth rate component, the north drift, the accelerometer bias, and the gyroscope drift.

3. System configuration

Figure 4 depicts the hardware configuration of the system. The volume of the system is 23 dm^3, and the weight of the system is about 20 kg. The complete system is composed of an inertially stabilized platform and an electronic cabin. The electronic cabin is equipped with eight PCB cards.

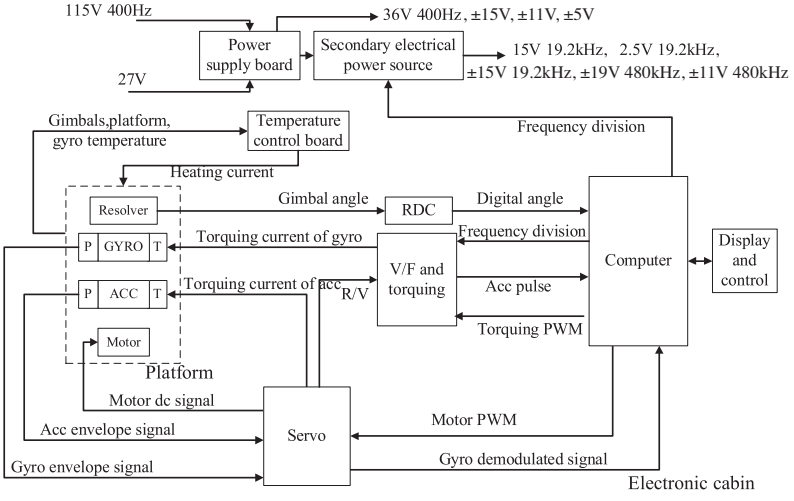

Fig. 4. The hardware configuration of the system.

The computer board adopts dual *digital signal processors* (DSP) as the core framework, the models of which are DSP TMS320F28335 and DSP TMS320F6747. The former is used to process the data measured by the sensors. It also calculates the control variables according to the control algorithm, and generates the *pulse-width modulation* (PWM) signals for the power amplifier. The latter carry out the initial alignment algorithm and the navigation calculation. To measure the gimbal angle, the resolver actual outputs are converted into digital signals using 19XSZ1411-S32-09H, which is a 19-bit-resolution tracking RDC, and its conversion accuracy is up to ±10″. The servo control board mainly includes accelerometer servo loop, gyroscope pickoff signal amplifier, shaping circuit, and power amplifier circuit. The digital conversion of the gyroscope pickoff signals is accomplished using a 4-channel ADS1274

Metrol. Meas. Syst., Vol. 26 (2019), No. 4, pp. 617–629
DOI: 10.24425/mms.2019.130566

with a maximum rate of 10.547 ksps, which can output 24 bits of data. The *Voltage to Frequency* (V/F) convertor and torqueing board are responsible for converting the acceleration signal to the digital pulse signal and converting the computer pulse to the corresponding current signal. The temperature control board is used to maintain stability of the gimbal temperature and the platform temperature. The operating temperature of gimbals is 60°C and its control precision is ±5°.The operating temperature of platform is 75° and its control precision is ±0.5°.

4. Experimental study

To verify the effectiveness of the proposed method, some experiments, such as the servo control loop, the initial alignment and the static navigation, have been carried out on a real rotational INS. Fig. 5 shows a photograph of the rotational INS and its experimental setup. The rotational INS is fed by a 27 V DC power supply and a 115 V, 400 Hz AC power supply, and the experimental data are collected by the host computer at a frequency of 100 Hz.

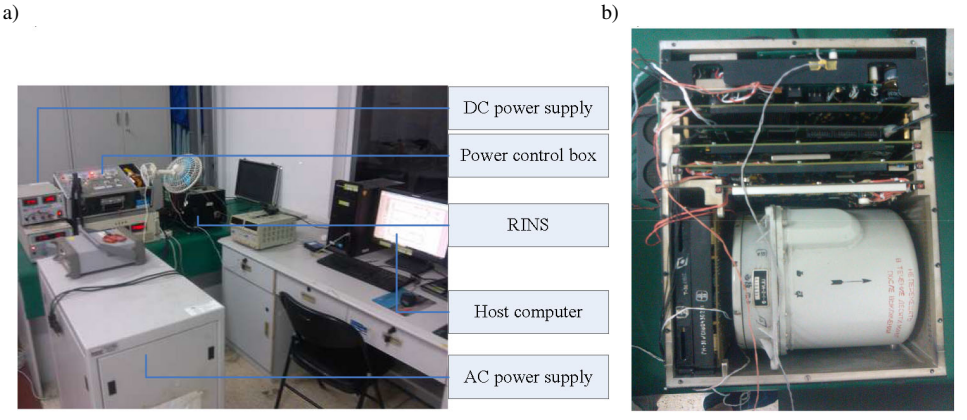

Fig. 5. The experimental setup of the rotational INS. a) The experimental equipment; b) the rotational INS.

4.1. Experiment 1: performance evaluation for control loop

The stabilized platform is designed to remove the effects of disturbances and provide a suitable navigation frame. At the same time, the platform can rotate bi-directionally along the z-axis at a rotation angular speed 1.2°/s. Hence, it not only needs to rotate smoothly, but also to respond to the following rotation command quickly. The *proportional-integral-derivative* (PID) controller is suitable for the control loop. The control frequency of loop is set to 1 kHz and the initial scope of PID parameters can be determined by the method of pole placement. The optimal parameter values have been achieved by the trial-and-error method. At the time of reversal, the initial value of integrator needs to be set based on the influence of friction torque. The curve of the rotation angle and the control error in the rotation cycle are shown in Fig. 6a. During the process of rotation, the torqueing current is 60 mA, which is shown in Fig. 6b.

The control error is less than 40″, and the dynamic error at the moment of reversal is less than 240″ during the rotation process. Fig. 6a proves that rotation has no obvious effect on the attitude calculation. The time of reversal is only tens of milliseconds, so the modulation is little

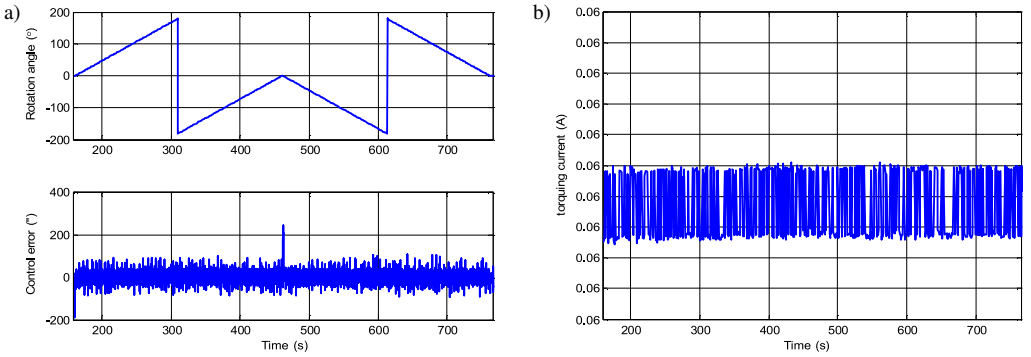

Fig. 6. The rotation test result of the stabilized platform.

affected by the dynamic error. The corresponding torqueing current of the precession angular velocity in Fig. 6b is measured by a 6–1/2 digital voltmeter and the rate of sampling is 1 s. Its relative standard deviation is 4.52e–5, and it proves the stability accuracy of power supply in the rotation process.

4.2. Experiment 2: alignment accuracy

To measure the repeatability of the alignment accuracy, the initial alignment experiment is carried out and repeated 6 times. The results of the alignment are listed in Table 2.

Table 2. The results of the alignment experiment.

Test Number	**Misalignment Angle (″)**			**North Drift And Gyroscope Drift (°/h)**		
	$\delta\phi_E$	$\delta\phi_N$	$\delta\phi_U$	ε_N	ε_x	ε_y
1	−24.3	−38.8	1035	0.0072	−0.0328	−0.0219
2	−33.0	−34.9	982	−0.0101	−0.0343	−0.016
3	−24.7	−38.1	1160	−0.0105	−0.0297	−0.0426
4	−27.1	−39.4	943	−0.0102	−0.0276	−0.0258
5	−19.9	−33.3	1202	−0.0118	−0.0231	−0.012
6	−21.5	−34.5	940	−0.008	−0.0199	−0.0097
MEAN	−25.08	−36.5	1043.7	−0.0072	−0.0279	−0.0213
STD	3.9	2.1	95.1	−0.00606	0.0047	0.01016

The estimation accuracies of the horizontal misalignment angle and the azimuth misalignment angle are approximately 3″ and 1.5′, respectively. The estimate accuracies of the north drift and the gyroscope drift in the sensitive axis are approximately 0.006°/h and 0.01°/h, respectively. Compared with the alignment accuracy of the original system, the azimuth alignment accuracy is improved by 6 times.

Metrol. Meas. Syst., Vol. 26 (2019), No. 4, pp. 617–629
DOI: 10.24425/mms.2019.130566

4.3. Experiment 3: static experiment in laboratory

To verify the effectiveness of the proposed alignment method, a complete laboratory experiment was carried out. In the initial alignment stage, the estimations of the misalignment angles and the gyroscope drifts were determined, and the results of the alignment are plotted in Fig. 7.

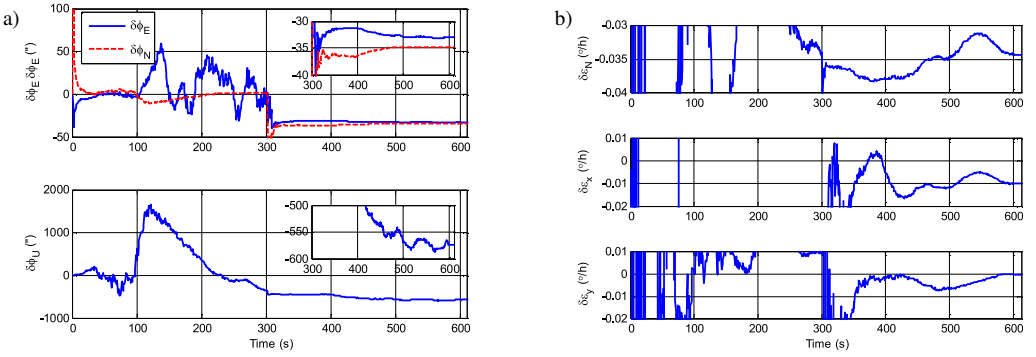

Fig. 7. The results of the estimation. a) Misalignment angle; b) gyroscope drift.

As depicted above, the estimations of the results can converge to the specified values, and the convergence results can be seen clearly in the graph insets in the figure. The estimation errors of the horizontal misalignment angles are less than 5″, and the azimuth misalignment angle is less than 1′. The estimation error of the north drift is less than 0.01°/h. Additionally, the input axis accelerometer bias and the gyroscope drift are estimated exactly. At the end of the alignment, the gyroscope drifts and the misalignment angles were compensated. Then, the system starts at the navigation state, and the platform rotates continuously.

Taking the influence of rotation into account, the acceleration of the measurement axis needs to be resolved through the rotation angle into the t-frame with the coordinate transformation in the process of the navigation calculation. The calculation of the velocity and position are inconsistent with an INS platform. Fig. 8 shows the experimental results of the velocity error and the position error. It can be seen that the maximum horizontal velocity error is about 0.6 m/s, and the maximum horizontal positioning error is less than 2,200 m. The position error CEP is 0.38 n mile/h. Compared with the original INS platform, the navigation performance of rotational INS based on a four-gimbal platform is improved by almost 5 times.

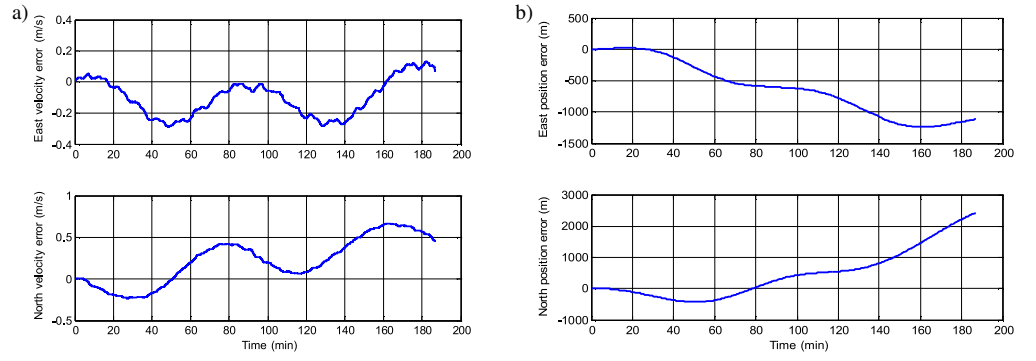

Fig. 8. The experimental results of the static navigation. a) Velocity error; b) position error.

5. Conclusions

In this paper, the technology of rotation modulation is applied to a four-gimbal inertially platform, and a new rotational INS is implemented. The proposed rotary upgrading method includes two parts; namely, the servo control loop and the initial alignment. The control loop not only has the function of level stability but can also rotate the platform bi-directionally and continuously along the vertical axis. The initial alignment model in the condition of rotation is established, and the recursive least squares method is used to estimate the state parameters. A set of experiments were carried out on a real rotational INS. The results of experiments indicate that the navigation accuracy of the system has reached 0.38 n mile/h (CEP) for 3 hours. The feasibility of rotary upgrading of the inertially stabilized platform has been verified.

References

[1] Hilkert, J.M. (2008). Inertially stabilized platform technology concepts and principles. *IEEE Control Systems*, 28(1), 26–46.

[2] Masten, M.K. (2008). Inertially stabilized platforms for optical imaging systems. *IEEE Control Systems*, 28(1), 47–64.

[3] Zhang, Q., Wang, L., Liu, Z.J., Feng, P.D. (2015). An accurate calibration method based on velocity in a rotational inertial navigation system. *Sensors*, 15(8), 18443–18458.

[4] Li, K., Gao, P.Y., Wang, L., Zhang, Q. (2015). Analysis and Improvement of Attitude Output Accuracy in Rotation Inertial Navigation System. *Mathematical Problems in Engineering*, 1, 1–10.

[5] Morris, M.K., Morray, S.G. (1983). Inertial Navigation. *Proc. of the IEEE*, 71(10), 1156–1176.

[6] Geller, E.S. (1968). Inertial System Platform Rotation. *IEEE Transactions on Aerospace & Electronic Systems*, 4(4), 557–568.

[7] Liang, A.C., Kleinbub, D.L. (1974). Drift Compensation and Acceleration Resolution for a Rotating Platform IMU. *Journal of Spacecraft & Rockets*, 11(8), 547–548.

[8] Ishibashi, S., Tsukioka, S., Yoshida, H. (2007). Accuracy improvement of an inertial navigation system brought about by the rotational motion. OCEANS 2007 – Europe. Aberdeen, Scotland, United Kingdom, *IEEE*, 1–5.

[9] Song, N., Cai, Q., Yang, G. (2013). Analysis and calibration of the mounting errors between inertial measurement unit and turntable in dual-axis rotational inertial navigation system. *Measurement Science & Technology*, 24(11), 5002–5012.

[10] Wang, L., Zhang, Q. (2014). Self-calibration method based on navigation in high-precision inertial navigation system with fiber optic gyro. *Optical Engineering*, 53(6), 064103–064111.

[11] Wang, L.C. Li, K., Chen, Y. (2017). Single-axis rotation/azimuth-motion insulation inertial navigation control system with FOGs. *Optics Express*, 25(25), 30956–30975.

[12] Sarma, S., Agrawal, V.K., Udupa, S. (2008). Instantaneous angular position and speed measurement using a DSP based resolver-to-digital converter. *Measurement*, 41(7), 788–796.

[13] Al-Emadi, N., Ben-Brahim, L., Benammar, M. (2014). A new tracking technique for mechanical angle measurement. *Measurement*, 54(8), 58–64.

[14] Zhang, C., Wang, L., Zhang, J. (2016). High precision locking control based on fiber optic gyro and photoelectric encoder for rotational inertial navigation system. *Ieice Electronics Express*, 13(20), 1–11.

[15] Fang, J., Yin, R., X., Lei. (2015). An adaptive decoupling control for three-axis gyro stabilized platform based on neural networks. *Mechatronics*, 27, 38–46.

Metrol. Meas. Syst., Vol. 26 (2019), No. 4, pp. 617–629
DOI: 10.24425/mms.2019.130566

[16] Ang, K.H., Chong G., Li, Y. (2005). PID control system analysis, design, and technology. *IEEE Transactions on Control Systems Technology*, 13(4), 559–576.

[17] Fang, L., Wei, W., Zhang, Z.Y. (2012). Motor rotation control method for rotation-modulation SINS. *Electric Machines & Control.*, 11, 17–21.

[18] Baritzhack, I.Y., Berman, N. (1988). Control theoretic approach to inertial navigation systems. *Journal of Guidance, Control and Dynamics*, 10(10), 1442–1453.

[19] Hung, J.C., White, H.V. (1975). Self-Alignment Techniques for Inertial Measurement Units. *IEEE Transactions on Aerospace & Electronic Systems*, 11(6), 1232–1247.

[20] Song, T., Li, K., Wang, L. (2017). A rapid and high-precision initial alignment scheme for dual-axis rotational inertial navigation system. *Microsystem Technologies*, 23(12), 1–11.

[21] Wang, X. (2009). Fast alignment and calibration algorithms for inertial navigation system. *Aerospace Science Technology*, 13(4), 204–209.

[22] Jiang, Y.F., Lin, Y.P. (1992). Error estimation of INS ground alignment through observability analysis. *IEEE Transactions on Aerospace & Electronic Systems*, 28(1), 92–97.

[23] Che, Y., Wang, Q., Gao, W. (2015). An Improved Inertial Frame Alignment Algorithm Based on Horizontal Alignment Information for Marine SINS. *Sensors*, 15(10), 1415–1419.

[24] Silva, F.O., Hemerly, E.M., Filho, W.C.L. (2016). On the error state selection for stationary SINS alignment and calibration Kalman filters – part I: Estimation algorithms. *Aerospace Science & Technology*, 61, 45–56.

[25] Liu, M., Gao, Y., Li, G. (2016). An Improved Alignment Method for the Strapdown Inertial Navigation System (SINS). *Sensors*, 16(5), 621–638.

[26] Wu, M., Wu, Y, Hu, X. (2011). Optimization-based alignment for inertial navigation systems: Theory and algorithm. *Aerospace Science & Technology*, 15(1), 1–17.

[27] Gao, W., Zhang, Y., Wang, J. (2015). Research on Initial Alignment and Self-Calibration of Rotary Strapdown Inertial Navigation Systems. *Sensors*, 15(2), 3154–3171.